AD-A141 107 THE USE OF NOVEL PROCESSING PROCEDURES FOR IMPROVING 1/1
THE OVERALL FATIGUE..(U) VIRGINIA UNIV CHARLOTTESVILLE
DEPT OF MATERIALS SCIENCE E A STARKE FEB 84
UNCLASSIFIED UVA/525638/MS84/101 AFOSR-TR-84-0357 F/G 11/6 NL

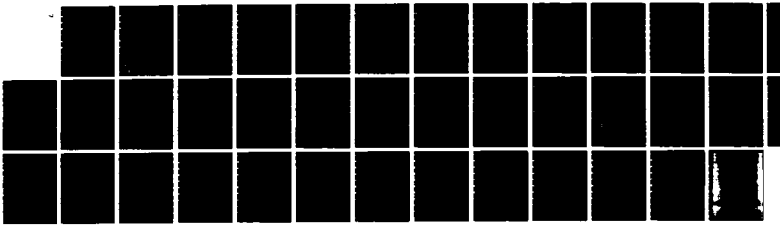

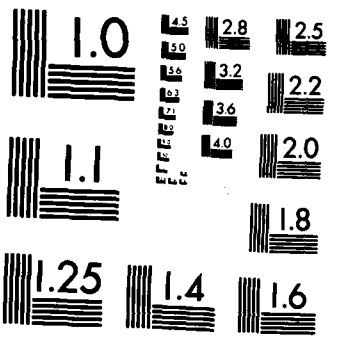

Annual Report

THE USE OF NOVEL PROCESSING PROCEDURES FOR IMPROVING OVERALL FATIGUE RESISTANCE OF HIGH STRENGTH ALUMINUM ALLOYS

Contract No. AFOSR-83-0061

Submitted to:

Air Force Office of Scientific Research/NE
Building 410
Bolling Air Force Base
Washington, D. C. 20332

Attention: Alan H. Rosenstein

Submitted by:

Edgar A. Starke, Jr.
Professor

Report No. UVA/525638/MS84/101
February 1984

SCHOOL OF ENGINEERING AND APPLIED SCIENCE

DEPARTMENT OF MATERIALS SCIENCE

UNIVERSITY OF VIRGINIA
CHARLOTTESVILLE, VIRGINIA 22901

Unclassified

SECURITY CLASSIFICATION OF THIS PAGE *(When Data Entered)*

REPORT DOCUMENTATION PAGE

READ INSTRUCTIONS BEFORE COMPLETING FORM

1. REPORT NUMBER: AFOSR-TR- 84-0357	2. GOVT ACCESSION NO.: AD-A141107
3. RECIPIENT'S CATALOG NUMBER:	
4. TITLE *(and Subtitle)*: THE USE OF NOVEL PROCESSING PROCEDURES FOR IMPROVING THE OVERALL FATIGUE RESISTANCE OF HIGH STRENGTH ALUMINUM ALLOYS	5. TYPE OF REPORT & PERIOD COVERED: Annual Scientific Report 1/1/83-12/31/83
	6. PERFORMING ORG. REPORT NUMBER: UVA/525638/MS84/101
7. AUTHOR(s): Edgar A. Starke, Jr.	8. CONTRACT OR GRANT NUMBER(s): AFOSR-83-0061
9. PERFORMING ORGANIZATION NAME AND ADDRESS: Department of Materials Science, University of Virginia, Thornton Hall, Charlottesville, VA 22901	10. PROGRAM ELEMENT, PROJECT, TASK AREA & WORK UNIT NUMBERS: 61102F 2306/A1
11. CONTROLLING OFFICE NAME AND ADDRESS:	12. REPORT DATE: January 30, 1984
	13. NUMBER OF PAGES: 33
14. MONITORING AGENCY NAME & ADDRESS *(if different from Controlling Office)*: Air Force Office of Scientific Research Directorate Electronics and Solid State Sciences, Bolling, AFB, Washington, D.C. 20332	15. SECURITY CLASS. *(of this report)*: unclassified
	15a. DECLASSIFICATION/DOWNGRADING SCHEDULE:

16. DISTRIBUTION STATEMENT *(of this Report)*

unlimited

Approved for public release; distribution unlimited.

17. DISTRIBUTION STATEMENT *(of the abstract entered in Block 20, if different from Report)*

18. SUPPLEMENTARY NOTES

19. KEY WORDS *(Continue on reverse side if necessary and identify by block number)*

Aluminum alloys, microstructure, ion implantation, fatigue

20. ABSTRACT *(Continue on reverse side if necessary and identify by block number)*

This program was initiated on January 1, 1983. Its objective is to develop an understanding of the mechanisms involved in the initiation and propagation of fatigue cracks in metals in order to optimize the microstructure of high strength aluminum alloys for overall fatigue resistance. The research conducted during this year was divided into three tasks.

Task I was concerned with the effects of slip character and grain size on the intrinsic material and extrinsic closure contributions to fatigue crack

DD FORM 1 JAN 73 1473 EDITION OF 1 NOV 65 IS OBSOLETE

unclassified

SECURITY CLASSIFICATION OF THIS PAGE *(When Data Entered)*

growth resistance of 7475. Special thermal mechanical processing procedures were developed to control the microstructural features of interest. The alloy was tested in the underaged and overaged conditions with grain sizes of 18 μm and 80 μm The fracture surfaces exhibited increased irregularity and planar facet formation with increased grain size, underaging, and tests in vacuum. These changes were accompanied by an increased resistance to fatigue crack growth. In air the 18 μm grain size overaged material exhibited relatively poor resistance to fatigue crack growth compared with other microstructural variants, and this was associated with a lower stress intensity for closure. All materials exhibited a marked improvement in fatigue crack growth resistance when tested in vacuum, with the most significant difference being ~1000X at a ΔK of 10 MPa $m^{\frac{1}{2}}$ for the 80 μm grain size underaged alloy. This improvement could not be accounted for by either an increase in closure or increased crack deflection and is most likely due to increased slip reversibility in the vacuum environment. The intrinsic resistance of the alloy to fatigue crack growth was microstructurally dependent in vacuum, with large grains and planar slip providing the better fatigue performance.

Task II was concerned with the use of the cyclic stress strain curve and a damage model for predicting fatigue crack growth thresholds. Fatigue crack initiation and fatigue crack propagation both involve the concept of cyclic accumulated damage. The details of the damage structure can be related to a material's cyclic stress strain response (CSSR). The CSS curve determined from the CSSR can be used to establish the onset of persistent slip bands (PSB's) which have been associated with the fatigue limit. We have equated the critical strain necessary to form PSB's to the strain at ΔK_{th}. The PSB concept was then used to modify the Chakrabortty fatigue crack propagation equation and to predict the intrinsic fatigue crack growth threshold. This concept allows an accurate prediction of ΔK_{th} and near threshold fatigue crack propagation when slip reversibility is minimal.

Task III is concerned with the effect of ion implantation on the low cycle fatigue response of 7475. Since fatigue crack initiation is a surface phenomenon and fatigue crack propagation is a bulk phenomenon, the fatigue properties may be optimized by production processes that develop microstructures resistant to FCI on the surface, and microstructures resistant to FCP throughout the bulk. Task I identified desirable microstructural features for FCP resistance. The idea of this task is to use ion implantation to produce a fine dispersion of nonshearable Al_6Fe particles near the surface. A high density of these particles should homogenize slip in the surface region and thus improve fatigue crack initiation resistance. Preliminary results indicate that this is a viable method of improving FCI resistance in 7475.

THE USE OF NOVEL PROCESSING PROCEDURES FOR IMPROVING THE OVERALL FATIGUE RESISTANCE OF HIGH STRENGTH ALUMINUM ALLOYS

AFOSR Annual Scientific Report
January 30, 1984

by

Edgar A. Starke, Jr.
Earnest Oglesby Professor of Materials Science
University of Virginia
Charlottesville, VA 22901

A1

This research was sponsored by the Air Force Office of Scientific Research Directorate of Electronics and Solid State Science under Research Grant Number AFOSR-83-0061

TABLE OF CONTENTS

ABSTRACT

This program was initiated on January 1, 1983. Its objective is to develop an understanding of the mechanisms involved in the initiation and propagation of fatigue cracks in metals in order to optimize the microstructure of high strength aluminum alloys for overall fatigue resistance. The research conducted during this year was divided into three tasks.

Task I was concerned with the effects of slip character and grain size on the intrinsic material and extrinsic closure contributions to fatigue crack growth resistance of 7475. Special thermal mechanical processing procedures were developed to control the microstructural features of interest. The alloy was tested in the underaged and overaged conditions with grain sizes of 18 μm and 80 μm The fracture surfaces exhibited increased irregularity and planar facet formation with increased grain size, underaging, and tests in vacuum. These changes were accompanied by an increased resistance to fatigue crack growth. In air the 18 μm grain size overaged material exhibited relatively poor resistance to fatigue crack growth compared with other microstructural variants, and this was associated with a lower stress intensity for closure. All materials exhibited a marked improvement in fatigue crack growth resistance when tested in vacuum, with the most significant difference being ~1000X at a ΔK of 10 MPa $m^{\frac{1}{2}}$ for the 80 μm grain size underaged alloy. This improvement could not be accounted for by either an increase in closure or increased crack deflection and is most likely due to increased slip reversibility in the vacuum environment. The intrinsic resistance of the alloy to fatigue crack growth was microstructurally dependent in vacuum, with large grains and planar slip providing the better fatigue performance.

Task II was concerned with the use of the cyclic stress strain curve and a damage model for predicting fatigue crack growth thresholds. Fatigue crack initiation and fatigue crack propagation both involve the concept of cyclic accumulated damage. The details of the damage structure can be related to a material's cyclic stress strain response (CSSR). The CSS curve determined from the CSSR can be used to establish the onset of persistent slip bands (PSB's) which have been associated with the fatigue limit. We have equated

the critical strain necessary to form PSB's to the strain at ΔK_{th}. The PSB concept was then used to modify the Chakrabortty fatigue crack propagation equation and to predict the intrinsic fatigue crack growth threshold. This concept allows an accurate prediction of ΔK_{th} and near threshold fatigue crack propagation when slip reversibility is minimal.

Task III is concerned with the effect of ion implantation on the low cycle fatigue response of 7475. Since fatigue crack initiation is a surface phenomenon and fatigue crack propagation is a bulk phenomenon, the fatigue properties may be optimized by production processes that develop microstructures resistant to FCI on the surface, and microstructures resistant to FCP throughout the bulk. Task I identified desirable microstructural features for FCP resistance. The idea of this task is to use ion implantation to produce a fine dispersion of nonshearable Al_6Fe particles near the surface. A high density of these particles should homogenize slip in the surface region and thus improve fatigue crack initiation resistance. Preliminary results indicate that this is a viable method of improving FCI resistance in 7475.

I. INTRODUCTION

Recent studies by the Air Force have shown that 50% of all material failures in aircraft are a result of fatigue (1). This high incidence of failures prompted the new safe-crack-growth approach for the design of new aerospace structural systems. However, accurate calculations require a knowledge of fatigue crack growth behavior under a wide variety of load and environmental conditions. Consequently, understanding the mechanisms involved in the initiation and propagation of fatigue cracks in metals is one of the key factors in designing aircraft that are safe, efficient, and economical. Since fatigue crack initiation is a surface phenomenon and fatigue crack propagation is a bulk phenomenon, the fatigue properties may be optimized by production processes that develop the desired microstructures for FCI resistance on the surface, and the desired microstructure for FCP resistance throughout the bulk. The objective of this program is to optimize the microstructure of high strength aluminum alloys for overall fatigue resistance, i.e., resistance to both FCI and FCP, through the use of new primary processing methods. Specifically, this research will identify those microstructural features that control the different aspects of fatigue, and establish methods for incorporating those features in a finished product.

II. SUMMARY OF PROGRESS DURING 1983

A. The Effect of Microstructure and Environment on Fatigue Crack Closure of 7475

The purpose of this study was to investigate the roughness-induced and oxide-induced crack closure behavior of 7475 aluminum alloy under different microstructural and environmental conditions. Emphasis was placed on the effect of grain size and deformation mode on crack closure of compact tension samples subjected to plane strain conditions in a vacuum and in a laboratory air environment.

The 7475 alloy used in this research was obtained as 2.5 inch thick plate from the Alcoa Technical Center. Starting with the 2.5 inch thick plate, two different intermediate thermomechanical treatments (ITMT's) were used to obtain the desired grain structure. They include solutionizing, overaging,

warm rolling, and recrystallization treatments. The large particles (~1 μm diameter) that result from the overaging treatment create strain concentrations during the warm rolling, and these deformation zones act as nucleation sites for recrystallization (2). Small grains, D_{eq} = 18 μm, were obtained by using a large amount of deformation and rapid heating to the recrystallization temperature. Large grains, D_{eq} = 80 μm, were obtained by using a small amount of deformation and slow heating to the recrystallization temperature. All heat treatments were conducted in a molten nitride salt bath except those associated with the rolling operation which were conducted in an electric air furnace. Samples were quenched in water from the recrystallization temperature, stretched approximately two percent to redistribute the residual quenching stresses, and naturally aged for three days. Samples for each grain size were artificially aged in an oil bath to obtain either an underaged or an overaged condition. Underaging 7475 produces coherent precipitates which are sheared by dislocations resulting in planar slip. Overaging produces incoherent precipitates which are looped and bypassed by dislocations resulting in wavy slip.

The yield strengths for the four experimental conditions (underaged and overaged, small and large grains) are listed in Table I. Reducing the grain size by factor of ~4 for the underaged condition increases the strength by 54 MPa. This increase is due to a small Hall-Petch contribution since the precipitates are sheared, the texture is random, and the slip length is determined by the grain size (3). However, the strength is independent of grain size for the overaged condition since the precipitates are looped and the slip length is determined by the interparticle spacing.

Table I. Yield Strength

18 μm Grain Size	Yield Strength (MPa)
underaged	505
overaged	455
80 μm Grain Size	
underaged	451
overaged	445

Fatigue Crack Growth Data

The fatigue crack growth response was investigated over the growth rate range $\sim 10^{-10}$ m/cycle to $\sim 10^{-6}$ m/cycle. The results obtained from 18 and 80 μm grain size material in the underaged and overaged condition and tested in laboratory are presented in Figure 1. For growth rates less than $\sim 10^{-8}$ m/cycle the overaged material exhibited less resistance to fatigue crack growth and lower "thresholds". The 18 μm grain size overaged material exhibited higher crack growth rates than the other materials investigated.

For tests carried out in vacuum there was a significant increase in fatigue crack growth resistance as illustrated in Figure 2. Data points are shown in this figure to illustrate the scatter associated with the tests. For the overaged alloy the crack growth rates at a ΔK of 7 MPa $m^{\frac{1}{2}}$ were reduced by a factor of ~10 in vacuum compared with an air tests environment. For the 80 μm grain size underaged alloy the fatigue crack growth resistance improved by a factor of >100 for a vacuum test environment. Both of the underaged alloys exhibited slower fatigue crack growth rates than the overaged alloys.

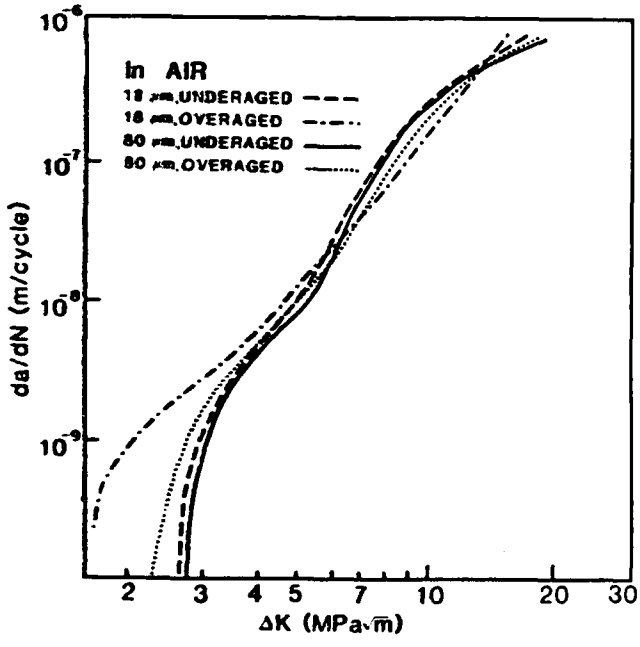

Fig. 1. FCGR's of the microstructural variants of 7475 tested in laboratory air.

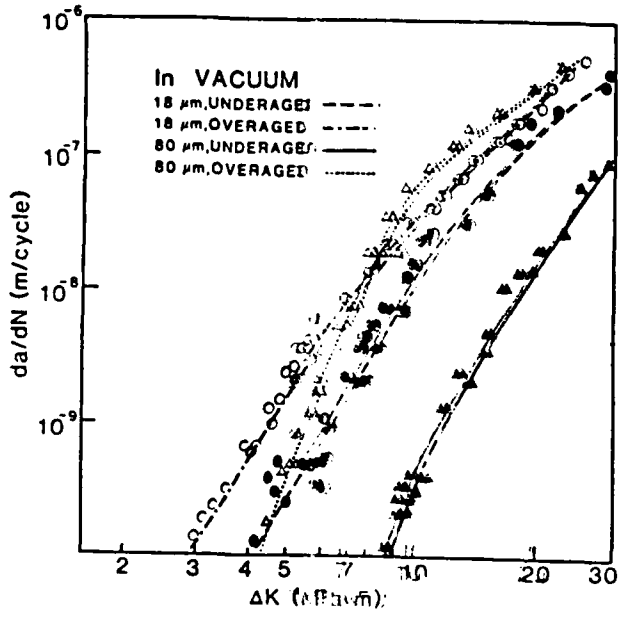

Fig. 2. FCGR's of the microstructural variants of 7475 tested in vacuum.

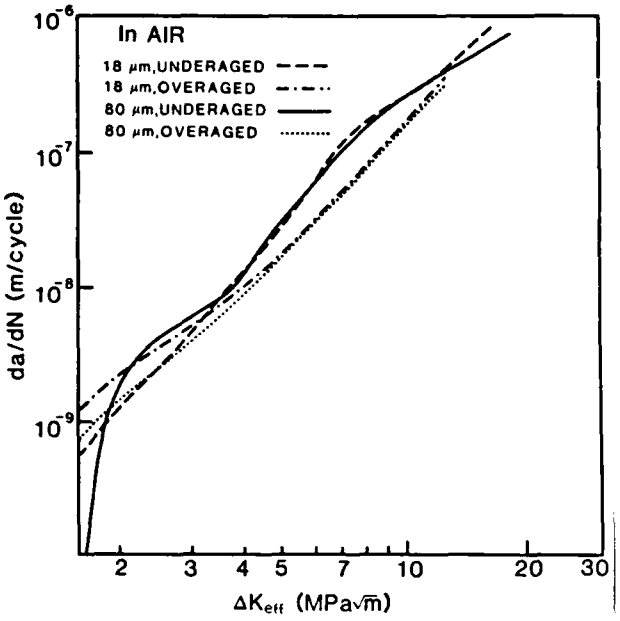

Fig. 3. FCGR's of the laboratory air tests as a function of the stress intensity range after correcting for closure.

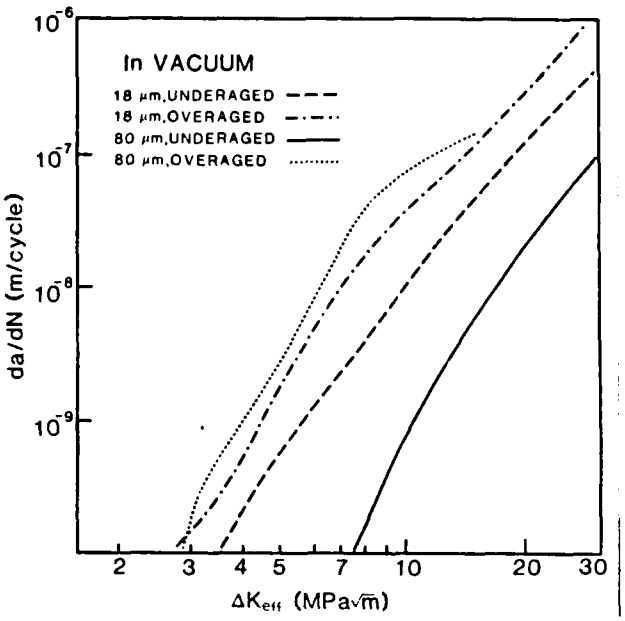

Fig. 4. FCGR's of the vacuum tests as a function of stress intensity range after correcting for closure.

The crack closure response of the CT specimens was measured and a load P_{op} was identified. By incorporating the load range P_{max} to P_{op} into the computation of ΔK a range of values of ΔK_{eff} was obtained. The results obtained for ΔK_{eff} are included in Figures 3 and 4 for the air and vacuum tests, respectively. In both air and vacuum, crack closure had occurred and the magnitude of the closure stress intensity was between 1 to 2 MPa $m^{\frac{1}{2}}$ for all materials. The fatigue crack growth curves in air were brought together by a ΔK_{eff} plot, but in vacuum the large difference in growth rate remained and the materials maintain a high degree of resistance to fatigue crack growth.

Examination of the fatigued but not completely broken test pieces at a macro level (magnification 25 times) revealed that the crack trajectory was nonplanar, and the extent of out of plane displacement of the crack increased with grain size and for the underaged condition. The most irregular crack path was observed in the 80 μm underaged alloy tested in vacuum. The fracture surface indicated a mixed mode of separation with facet formation on crystallographic planes and transgranular ductile separation with some striation formation. Facet formation occurred in both air and vacuum tests and in the underaged and overaged alloys.

Discussion

The present results are consistent with earlier studies that showed that slip character (4), and grain size (5) can have a pronounced effect on the fatigue crack growth behavior of age hardenable aluminum alloys. When the strengthening precipitates are coherent with the matrix (underaged condition) they are sheared by dislocations promoting coarse planar slip and inhomogeneous deformation. This favors fracture along slip planes and the occurrence of zigzag crack growth and crack branching. When the strengthening precipitates are incoherent with the matrix (overaged condition), they are looped and bypassed by dislocations promoting more homogeneous deformation and reducing crack tortuosity. A reduction in grain size (by enhancing multiple slip at low ΔK's) (5) and an aggressive environment (by decreasing the plasticity needed for fracture) (6) can also reduce crack tortuosity although the oxides formed in air can have an opposite effect on crack growth rates by contributing a closure component. The slower crack growth rates associated with planar slip and large grains have been attributed to: (a) slip being more reversible, (5), (b) the tortuosity of the crack path (4), (c) the ΔK of zigzag and branched cracks being smaller than the ΔK calculated assuming a single crack normal to the stress axis (4), and (d) enhanced closure associated with increased surface roughness (7).

A reduction in grain size, overaging, and an air environment reduces the reversibility of slip and crack tortuosity. Consequently, it is not surprising that the 18 μm grain size, overaged material had the poorest fatigue resistance of all the conditions studied. A comparison of Figures 1 and 3 suggests that the differences in fatigue crack growth rates for the various materials may be related to the difference in the extent of crack closure that they exhibited in the air environment. However, this is probably an oversimplification of microstructure-closure-FCP relationship. Figure 5 shows the variation in U with ΔK for all materials tested in laboratory air, where

$$U = \frac{K_{max} - K_{cl}}{\Delta K} \quad . \qquad [1]$$

It is obvious that the difference in closure between the 18 μm grain size overaged material and the other microstructural variant is essentially constant up to a ΔK of $\sim$8 MPa $m^{\frac{1}{2}}$ although the growth rates converge at $\sim$4 MPa $m^{\frac{1}{2}}$. This may be due to an environmental contribution which is independent of closure. Lin and Starke (8,9) have shown that environmentally enhanced crack growth is greater for underaged than for overaged Al-Zn-Mg alloys and may also increase with increasing grain size. This could account for the convergence in crack growth curves even though the difference in closure contribution is maintained. One other observation should be noted here. The closure contribution is smaller

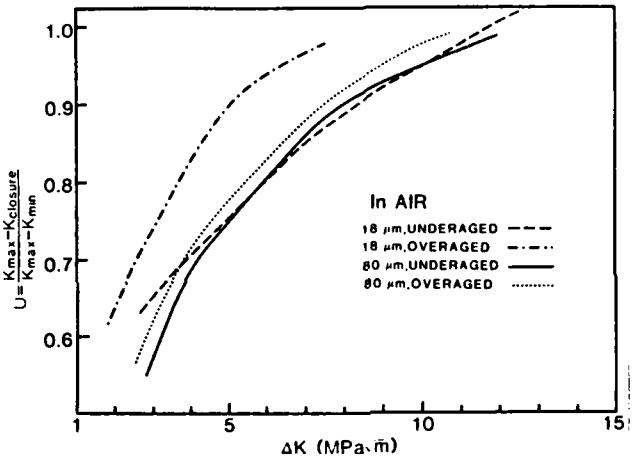

Fig. 5. Comparison of the closure as a function of ΔK for the microstructural variants tested in air.

for the overaged than for the underaged small grain size material. Vasudévan and Suresh (10) have shown that the oxide layer formed during fatigue of 7075 in air is thicker for overaged than for underaged materials. This fact in conjunction with our results indicates that the measured closure for the underaged alloy is not primarily due to oxides.

The creation of the asperities which resulted in closure can be attributed to out of plane crack trajectories (11), i.e., roughness induced closure. The magnitude of the out of plane crack trajectory may be related to the ratio of the true crack length to the projected crack length, which for lack of

a better term, we will define as the roughness parameter. The order of crack growth resistance is directly related to the magnitude of the closure component (Figure 5) and the roughness parameter (Table II).

Table II. Roughness Parameter

Condition	True Length/Projected Length	
	Vacuum	Air
18 μm grain size		
UA	1.13	1.14
OA	1.05	1.05
80 μm grain size		
UA	1.67	1.18
OA	1.09	1.09

The results of the vacuum studies were quite unlike those in air in that the differences in growth rates for the various materials could not be accounted for by closure effects (Figure 4). The influence of environment and in particular the improvement in fatigue crack growth resistance in vacuum has been observed in a range of aluminum alloys (4,5,8,9,12). The extent of the improvement depends on aging condition and grain size, with the most significant improvements derived from coarse grained material in an underaged condition. Examination of Figure 2 shows that a similar response was achieved for the 7475 alloy. One factor which may account for this is the marked extent of slip reversibility in the underaged material compared with the multiple slip situation in the overaged material. An indication of the slip reversibility may be that the closure for the large grained UA material in vacuum and in air was the same (compare the U values in Figures 5 and 6 at ΔK = 10 MPa $m^{\frac{1}{2}}$) even though the fracture surface from the vacuum test was considerably rougher than the air test. Reversible slip would decrease the Mode II displacement during unloading and therefore the component of roughness induced closure. Reversible slip should also increase the number of cycles necessary to produce unit crack extension along a Mode II plane.

The crack closure that occurred in vacuum is represented in Figure 6 as variations in U, for the different materials, as a function of ΔK. The 18 μm overaged alloy showed no detectable closure at a ΔK of 5 MPa $m^{\frac{1}{2}}$. The increase of K_{cl} in air for this overaged material may be a consequence of oxide layer build-up (oxide induced closure) or alternately a consequence of a more irregular crack path and to microstructurally originated asperities, although the latter appear unlikely since the fracture surfaces and roughness parameter from the air and vacuum tests were similar for this microstructure. Figure 6 also shows that the closure contribution was greater for both the underaged and overaged 80 μm grain size than for the underaged 18 μm grain size material. The closure is most likely associated with microstructurally originated asperities that result from the out of plane crack trajectories and Mode II displacements (roughness induced closure) (11) particularly since alternatives such as oxides and plasticity induced closure are absent for the vacuum tests at low ΔK levels. Although the roughness parameter of the underaged 18 μm grain size material was slightly larger than that for the overaged 80 μm grain size material, the closure was smaller. This is probably a consequence of slip being more reversible in the UA material.

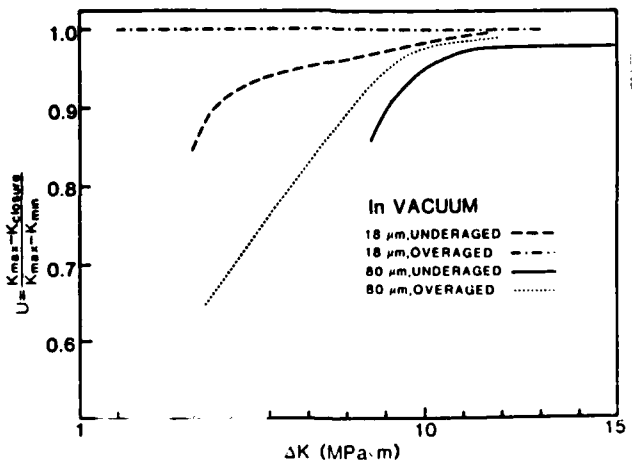

Fig. 6. Comparison of the closure as a function of ΔK for the microstructural variants tested in vacuum.

The results in Figure 4 show that a marked difference exists between the intrinsic resistance of the 7475 alloy in the overaged and underaged condition. At a ΔK of 10 MPa $m^{\frac{1}{2}}$ the 80 μm underaged alloy exhibits a growth rate nearly 100X slower than the 80 μm overaged alloy, and both underaged alloys exhibit greater fatigue crack growth resistance than the overaged alloys. An examination of the fractographs and crack profiles showed that the underaged 80 μm grain size material exhibited marked surface irregularities and the crack advance involved both Mode I and II crack tip opening. Suresh (13) has suggested the folowing relationship for a deflected crack with Mode II component

$$\frac{d\bar{a}}{dN} = \left(\frac{D\cos\Theta + S}{D + S}\right)\left(\frac{d\bar{a}}{dN}\right) \qquad [2]$$

Θ denotes the angle of deflection, D the distance over which the tilted crack advances along the kink, and S the distance over which linear (Mode I) crack growth occurs. $(d\bar{a}/dN)$ is the measured averaged growth rate of a deflected crack in each segment and (da/dN) the growth rate of an undeflected crack. For the 80 μm underaged alloy tested in vacuum Θ = 70 deg and S = 0.1 D. Using Suresh's analysis, the deflected crack has a 2.5 times slower growth rate compared with the undeflected crack. While a contributing factor, crack branching does not appear to be the complete explanation of the wide variations in fatigue crack growth rate presented in Figure 4.

There are several other possible explanations of this behavior, but these are qualitative in character. Extensive out of plane crack growth with significant proportions of the crack advance under Mode II displacements was observed. If the crack extension rates for equivalent displacements are less under Mode II than Mode I, then the crack profiles developed in the 80 μm underaged alloy would lead to a decrease in growth rate. A further point for consideration is the interaction of the fracture planes behind the crack tip. On the unloading part of the cycle the cracks may be pushed into firm contact as they attempt to slide over one another due to the reversible nature of the Mode II displacement for this microstructure. Only the 80 μm grain size material maintains the reverse and maximum plastic zone size less than

the grain size at ΔK = 10 MPa $m^{\frac{1}{2}}$. Sliding contact may well lead to friction welding of part of the crack faces with a subsequent reduction in the crack extension force. The friction welding together of fresh metal surfaces in vacuum under nonfatigue conditions is a well-established phenomenon. The extent of its role in this particular case will be quantified during 1984.

Some observations on the differences between the air and vacuum tests are appropriate. The 80 μm grain size underaged alloy has a growth rate 1000 times slower in vacuum than air at a ΔK of 10 MPa $m^{\frac{1}{2}}$. This outstanding difference is related to the factors previously discussed in relation to the behavior in vacuum. The other alloys exhibit the modest differences in fatigue crack growth rate up to a factor of 10 that might be expected for air and vacuum tests. The decrease in fatigue crack growth rate in vacuum may be attributed to the absence of an oxide layer in the crack tip region allowing slip reversibility to inhibit more effectively the crack extension process. The vacuum also excludes the presence of water vapor and other gases which could lead, for example, to hydrogen embrittlement of the material in the crack tip process zone and subsequently increase in the crack extension rate.

B. The Use of the Cyclic Stress Strain Curve and a Damage Model for Predicting Fatigue Crack Growth Thresholds.

It is the goal of the fatigue researcher to develop an understanding of fatigue mechanisms to the degree that would allow an accurate prediction of the life of a component under a given set of experimental conditions. This includes a conceptional awareness of fatigue as an evolutionary process involving both micro- and macro-instabilities which lead to final failure. Classically, the fatigue process is divided into two stages, crack initiation and subsequent crack propagation, and researchers normally focus on one aspect or the other with little or no attempt to wed the two. This approach may be partly due to the increased emphasis on damage tolerant design which most often assumes a preexisting flaw or crack, and this eliminates the initiation stage.

Both stages of fatigue involve the concept of "damage" which leads to the initiation of a crack and which develops in the plastic zone at the crack

tip and ultimately results in fracture. There are different views as to the definition of this "damage" (14), and some of these have been expressed at a recent ASTM conference on the subject (15). However, in the context of this report, fatigue damage will be associated with the dislocations, substructure, slip bands, etc., that develop under cyclic loading. Consequently, knowledge of the basic mechanisms in the cyclic deformation of metals and alloys is a necessary prerequisite in elaborating a fatigue damage concept. The details of the damage structure that develops during cyclic loading has been extensively studied in the past 25 years and discussed in a number of review articles (16-18). The objective of this task was to use the fundamental concepts established by these studies to develop a model which predicts fatigue crack growth thresholds.

Modeling Fatigue Crack Growth Thresholds

The fatigue thresholds stress intensity can be considered to consist of a closure component, $\Delta K^{c}_{th_i}$, and a component related to the material's resistance to crack extension, ΔK_{th}, giving (19)

$$\Delta K_{th} \text{ (measured)} = \Delta K^{c}_{th} + \Delta K^{i}_{th}. \qquad [3]$$

ΔK^{c}_{th} is the stress intensity range which must be exceeded to overcome the extrinsic influence on crack extension and depends on a closure associated with residual stresses (20), oxides (21), surface roughness (22,23), etc. ΔK^{i}_{th} is the stress intensity range which must be exceeded to overcome the intrinsic resistance of the material to crack extension and depends on elastic modulus, cyclic hardening exponent, cyclic yield strength, slip length (grain size), slip mode, slip reversibility, and grain orientation/deflection. We will be concerned with the intrinsic component of the fatigue threshold, but will exclude the contribution due to grain orientation/deflection which has been treated in detail by Suresh (24). Any comparison of the model developed here with experimentally measured ΔK_{th} must be made after the measured value has been corrected for both closure and deflection.

Intrinsic effects on FCP resistance are treated in the Chakrabortty

model (25). Our extension of that model to include the threshold concept is based on the premise that there is a plastic strain amplitude $(\Delta\varepsilon_p/2)_{th}$ below which deformation is reversible and fatigue damage is not accumulated (26). For plastic strain amplitudes greater than or equal to $(\Delta\varepsilon_p/2)_{th}$, fatigue damage is accumulated and crack nucleation and extension can occur. We equate $(\Delta\varepsilon_p/2)_{th}$ to the critical strain necessary to form PSB's, and incorporate $(\Delta\varepsilon_p/2)_{th}$ in the Chakrabortty equation giving

$$\frac{da}{dN} = 2 \sum_n \bar{\rho}_n^{-}[(\Delta\varepsilon_{pn} - \Delta\varepsilon_{p_{th}})/2\varepsilon_f^{-}]^{-1/c}. \qquad (4)$$

Our assumptions are supported by the evidence that cracks nucleate in PSB's and early crack extension occurs crystallographically along PSB's. These PSB's reform and develop continuously ahead of the crack tip (27). Near-threshold crack extension in deeply-notched samples, e.g., compact tension specimens, has also been observed to occur by the crystallographic stage I shear mode (28-30), with a transition to the noncrystallographic stage II mode at higher da/dN and ΔK's (Paris regime) (31,32).

Figure 7 shows the effect of variations in $(\Delta\varepsilon_p)_{th}$ on the crack growth rates, as a function of ΔK. There is little or no effect for crack growth rates greater than 10^{-7}m/cycle for this example. The curves were obtained using equation [4] and LCF data from an underaged Al-Zn-Mg alloy having only shearable precipitates (33). Consequently, the slip length was controlled by the grain size and $\bar{\rho}^{-}$ was taken to equal the grain diameter, D = 15 μm, for Fig. 7a. Figure 7b was obtained similarly using a larger grain size to illustrate the interactive effects of $(\Delta\varepsilon_p)_{th}$ and $\bar{\rho}^{-}$. By equating ΔK_{th} to the stress intensity factor corresponding to a crack growth rate, da/dN, of 10^{-10}m/cycle, and plotting ΔK_{th} versus $(\Delta\varepsilon_p)_{th}$, we can schematically show the influence of $(\Delta\varepsilon_p)_{th}$ on ΔK_{th} for two different grain sizes, Fig. 8.

Grain size and strength have been previously shown to effect ΔK_{th}, but the dependence of ΔK_{th} on these variables is complex and somewhat controversial (34). Many investigators have observed an increase in ΔK_{th} with grain size while others have observed an opposite effect (35). Beevers (19) showed that ΔK_{th} increased with strength for a range of medium to high strength metals while Minakawa and McEvily (36) showed an inverse dependence for a similar

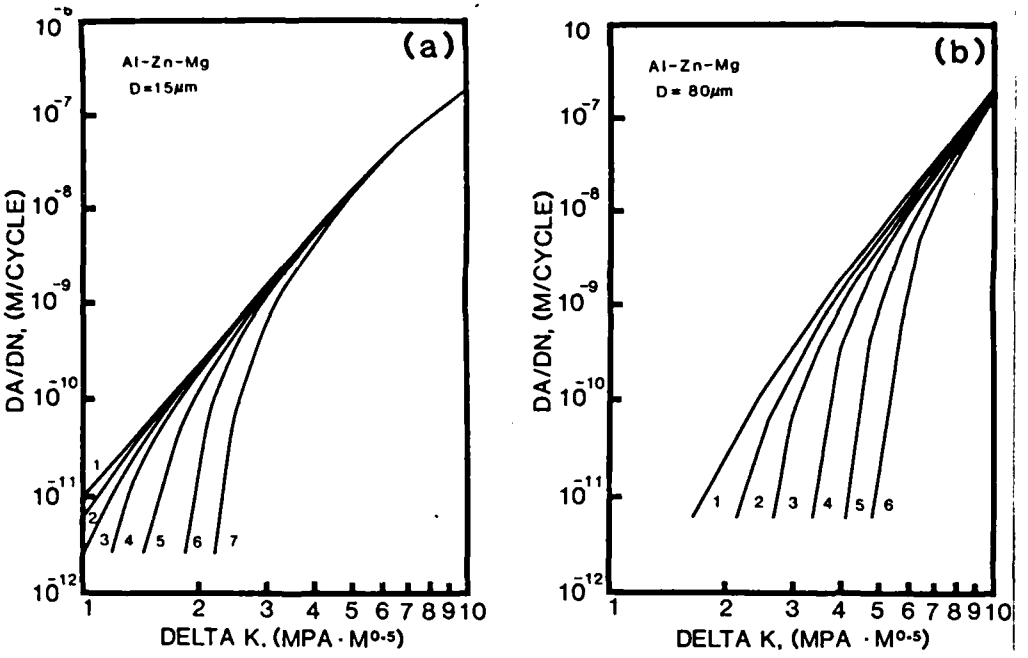

Fig. 7. Schematic of the crack growth rates as a function of ΔK for various $(\Delta\varepsilon_p)_{th}$ beginning with 2.5×10^{-5} and increasing in multiples of 2 to 10^{-3}. (a) for a slip length of 15 μm and (b) for a slip length of 80 μm.

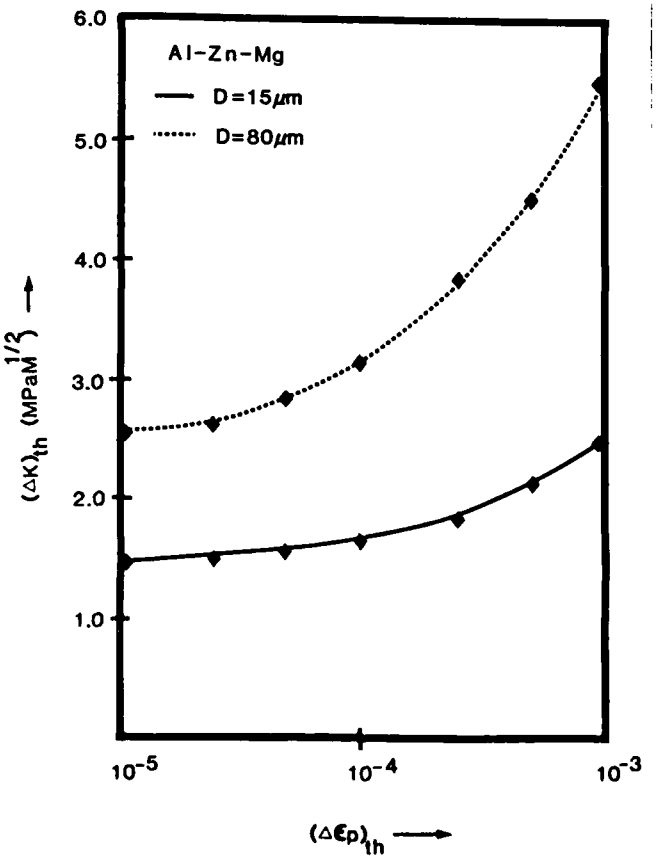

Fig. 8. Schematic representation of the predicted change in ΔK_{th} with $(\Delta\varepsilon_p)_{th}$ for two different slip distances.

series of alloys. The relationship between threshold and grain size, as predicted by eq. [4] using the LCF data of Heikkenen (33) and a $(\Delta\varepsilon_p)_{th}$ of 10^{-4}, is schematically represented in Fig. 9a. Similarly, the relationship between the threshold and yield strength is shown in Fig. 9b. The predicted change in ΔK_{th} with grain size corresponds almost exactly to that observed by Lindigkeit et al. (37) in vacuum tests for similar Al-Zn-Mg alloys having a constant yield strength. In most cases an increase in grain size is accompanied by a concurrent decrease in strength as described by the Hall-Petch relationship (38,39). Since such a simultaneous change would effect the threshold in opposite directions, the confusion in the literature may be associated both with failure to control each parameter individually, and different grain size-strength relationships for different alloys.

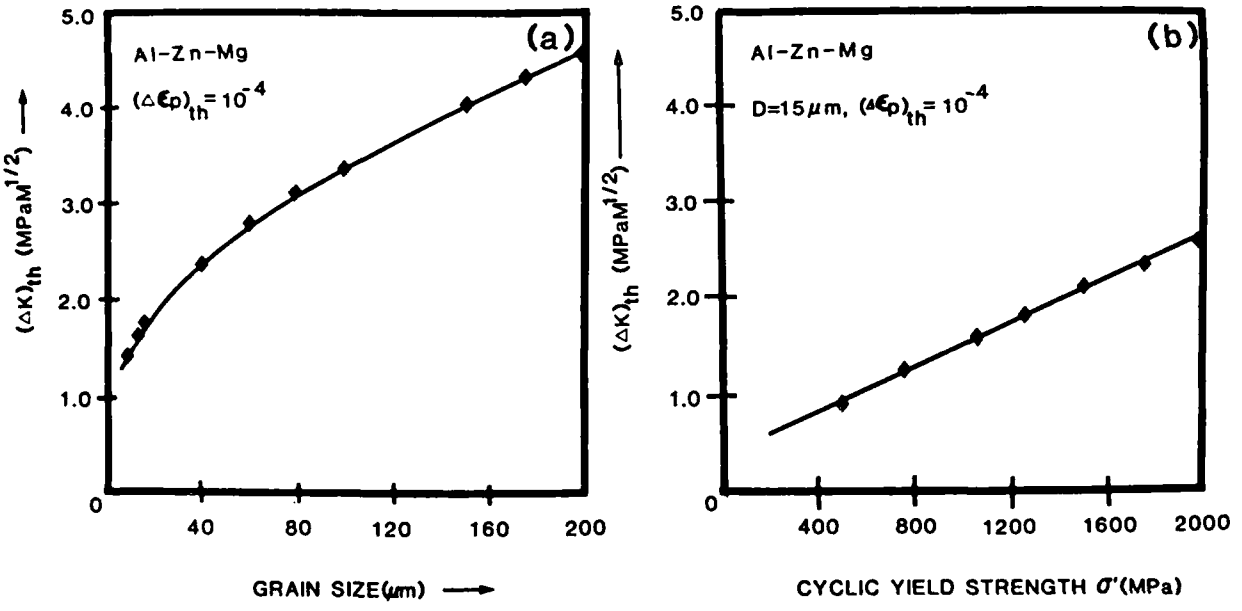

Fig. 9. Schematic representation of the predicted change in ΔK_{th} with (a) grain size and (b) cyclic yield strength.

In most materials strength is associated with a combination of mechanisms, e.g., solid solution, precipitates, dispersoids, grain and subgrain boundary effects. Collectively, the contribution of each mechanism is somewhat less than anticipitated from an individual basis (3). Consequently, the Hall-Petch relationship may be rewritten as (40)

$$\tau_y = m\tau_o + (m^2 \tau^* r^{\frac{1}{2}})d^{\frac{1}{2}} \qquad [5]$$

where m is an orientation factor related to the number of slip systems available, τ_o is the friction stress on a single dislocation, τ^* is the critical shear stress required to activate a dislocation source and r and is a measure of separation of the source from the nearest dislocation pileup. τ_o depends on the various matrix hardening mechanisms, and a large τ_o reduces the grain size contribution to the strength. For example, Fig. 9 schematically represents the yield stress-grain size relationship for two different alloys, A and B. An increase in grain size of Δd_A for alloy A results in a decrease in strength equal to $\Delta\sigma$. However, a much larger increase in grain size, Δd_B, is required for the same decrease in strength for alloy B. Consequently, an examination of the strength-ΔK_{th} relationship may show a positive effect for alloy A (strength dominance) and a negative effect for alloy B (grain size dominance).

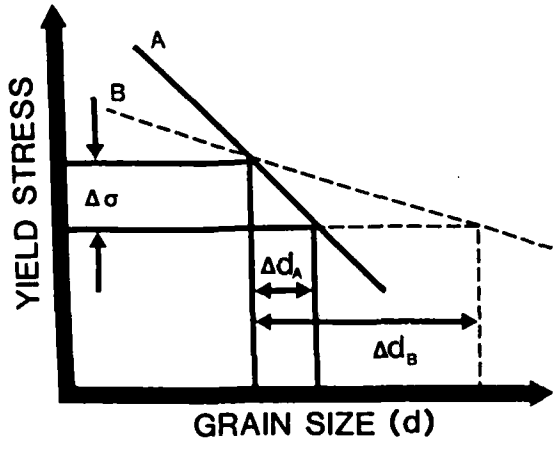

Fig. 10. Schematic representation of the yield stress-grain size relationship for two materials having different Hall-Petch effects.

Comparisons With Experimental Measurements

Low cyclic fatigue data was obtained for a polycrystalline Al-6Zn-2Mg-0.2Zr alloy having a recrystallized grain size of 15 μm and a random texture. This composition was selected so only shearable precipitates would be present in the underaged condition. Measurements were made in laboratory air (relative humidity ~60%), dry air (maximum H_2O content, 3 ppm), and vacuum (10^{-6} torr) environments for underaged specimens and dry air for overaged specimens. FCP tests were performed on compact tension specimens for the same aging conditions in similar environments. FCGR's were experimentally corrected for closure which was measured at 0.2 Hz from plots of load versus displacement using a clip-on displacement gage. The details of sample preparation and experimental procedures are given elsewhere (33).

Table III. Cyclic and Microstructural Parameters Used for ΔK_{th} and FCGR Prediction

Alloy	Test Environment	|c|	ε_f' (EFP)	n' (RNP)	K' (MPa) (RKP)	ρ' (m) (RHO)	E (MPa)
Underaged	Lab. Air	0.56	0.15	0.046	1058	15×10^{-6}	7×10^4
Underaged	Dry Air	0.58	0.20	0.048	1058	15×10^{-6}	7×10^4
Underaged	Vacuum	0.58	0.22	0.048	1058	15×10^{-6}	7×10^4
Overaged	Dry Air	0.65	0.32	0.065	1100	15×10^{-6}	7×10^4

The cyclic and microstructural parameters used for calculated FCGR's and ΔK_{th} prediction are given in Table III. There was no significant difference in the LCF results for the different environments for the underaged alloy. The CSS curve for this aging condition is given in Fig. 11, as saturation stress versus the log of the plastic strain amplitude, and compared to the results obtained by Renard et al. (41) for a similar alloy and aging treatment. Equipment limitations prevented us from making measurements below a plastic strain amplitude of 10^{-4} but Renard et al.'s data covers the range 8×10^{-7}

to 10^{-2}. There is very good agreement between the region of overlap with the stress amplitudes from our measurements being slightly higher. This is probably associated with the presence of zirconium, a small grain size and a lightly higher Hall-Petch effect for our alloy. There is a significant change in slope at $\Delta\varepsilon_p/2$ of 10^{-4} which may be associated with the regime I-regime II transition. This contention is supported by Wilhelm's (42) studies on underaged Al-Zn-Mg crystals. He found that PSB's did not form at $\gamma_p < 10^{-4}$ but did form at slightly higher values. Consequently, we will equate $(\Delta\varepsilon_p/2)_{th}$ to $10^{-4}/2.24$ for this alloy system. Closure-compensated FCGR's of the underaged alloy were corrected for crack deflection using the procedures described by Suresh (24) and given in Table IV. No deflection correction was required for the overaged alloy.

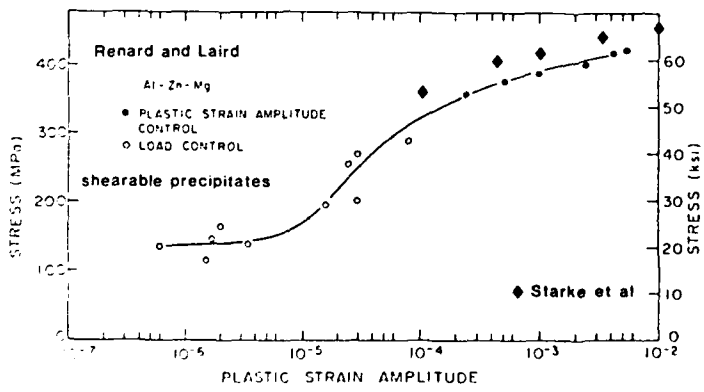

Fig. 11. CSSC for underaged Al-Zn-Mg alloys.

Table IV. Crack Deflection Corrections for the Underaged Al-Zn-Mg Alloys

Environment	Deflection (Θ)	Weight ($\frac{D}{D+S}$)	$(d\bar{a}/dN)/(da/dN)$	$\Delta K_{eff}/\Delta K_I$
Lab Air	5^o	0.5	0.998	1
Dry Air	20^o	0.5	0.97	0.98
Vacuum	40^o	0.5	0.88	0.94

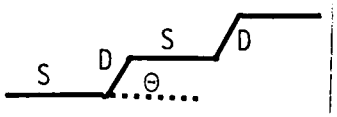

single kinked crack

$$\left(\frac{d\bar{a}}{dN}\right) = \left(\frac{D\cos\Theta + S}{D + S}\right)\left(\frac{da}{dN}\right), \quad \Delta K_I \quad \Delta K_I\left[\frac{D\cos^2\left(\frac{\Theta}{2}\right) + S}{D + S}\right]$$

$\frac{d\bar{a}}{dN}$: measured FCG rate (apparent)

$\frac{da}{dN}$: FCGR for a straight crack at the same ΔK

ΔK_I: nominal ΔK for mode I crack

$\overline{\Delta K_I}$: the average stress intensity range in each segment

Comparisons of the calculated intrinsic and closure-deflection-corrected experimental FCGR curves for the underaged Al-Zn-Mg alloy are given in Fig. 12a-c. The parameters used for the calculated values are listed on each figure. The notation was defined in Table III with the exception of $(\Delta\varepsilon_p)_{th}$ which is DEPT. There is relatively good agreement for the laboratory air and dry air curves. However, a large difference exists between the calculated and measured vacuum data. We believe the discrepancy may be associated with slip reversibility. The decrease in fatigue crack growth rate in vacuum may be attributed to the absence of an oxide layer in the crack tip region allowing slip reversibility to more effectively inhibit the crack extension process. The model developed in this paper does not directly consider slip reversibility effects which may be significant for underaged materials which deform by planar slip. Although such effects should also occur in LCF specimens and therefore be included in the model, reversibility is probably more extensive when the fatigue crack propagation reversed plastic zone (FCP-RPZ) is contained in one grain (near threshold) than in the polycrystalline LCF specimen. For the latter case strain is fairly uniform through the sample thickness and grain boundary effects can decrease slip reversibility. Consequently, the $(\Delta\varepsilon_p/2)_{th}$ required for PSB formation may be somewhat smaller than that required for crack extension in the compact tension sample. Since overaging decreases slip reversibility (there is an associated decrease in precipitate coherency), a close correlation should exist between calculated and measured values for overaged alloys if slip reversibility is responsible for the discrepancy. Figure 13 shows this to be the case.

The results obtained in Task 1 offerred the opportunity of comparing calculated and measured values for the commercial alloy 7475 whose nominal composition is Al-6Zn-2.4Mg-1.6Cu-0.2Cr. Figure 14 shows the results of this analysis for vacuum FCP tests. Measured and calculated ΔK_{th} values are tabulated in Table V along with those obtained for the Al-Zn-Mg alloy. There is a smaller discrepancy between measured and calculated FCG's for the underaged alloy, Fig. 14a, than observed for the underaged Al-Zn-Mg alloy of Fig. 12. this is probably due to the presence of the incoherent Cr-rich dispersoid in 7475 which should decrease slip reversibility. The calculated and measured values

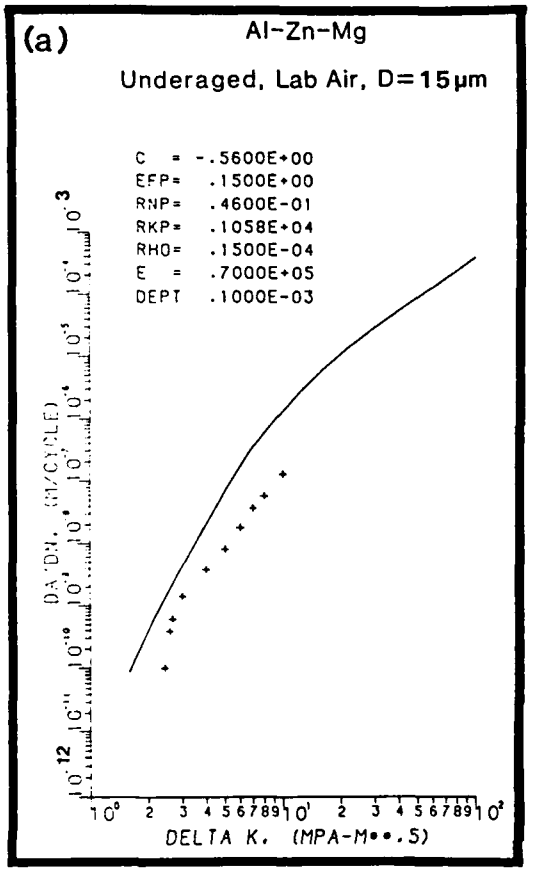

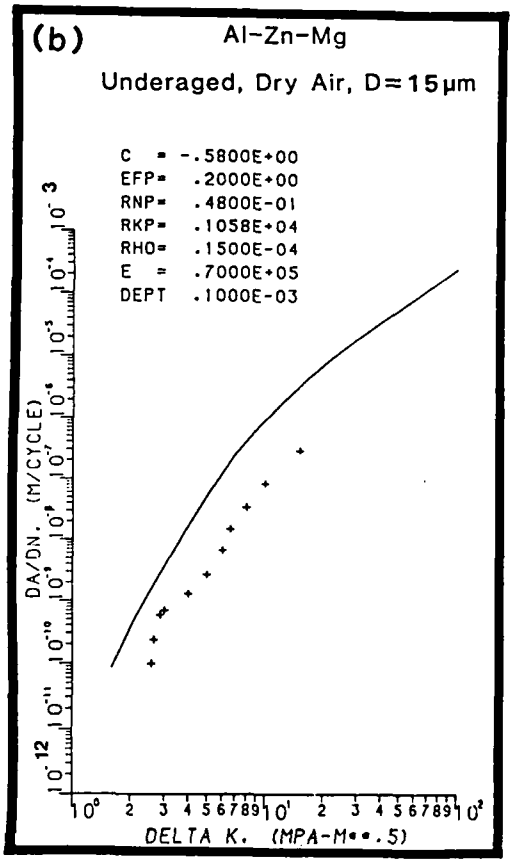

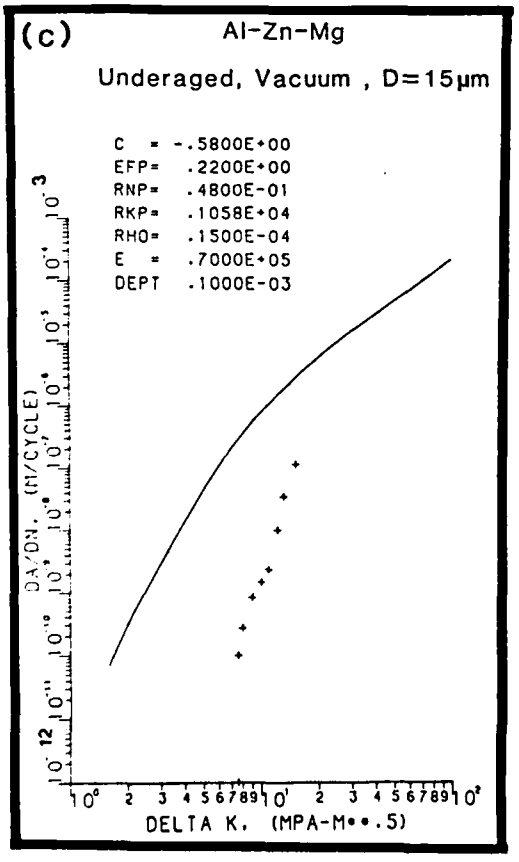

Fig. 12. Predicted and measured (+) crack growth data for underaged Al-Zn-Mg tested in (a) lab air, (b) dry air and (c) vacuum. Measured values have been corrected for closure and crack deflection.

were coincident, however, for the overaged condition. As mentioned previously, slip reversibility should be minimal for this condition.

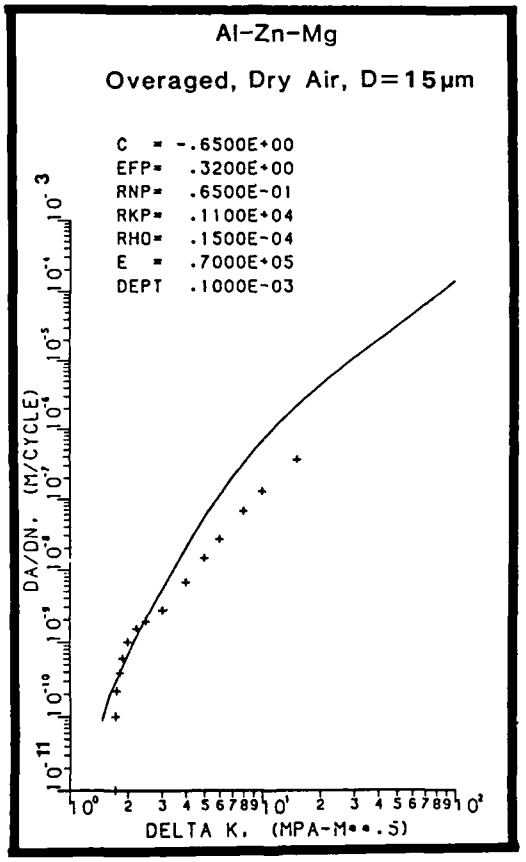

Fig. 13. Predicted and measured (+) crack growth data for overaged Al-Zn-Mg tested in lab air. Measured values corrected for closure--no deflection correction was necessary.

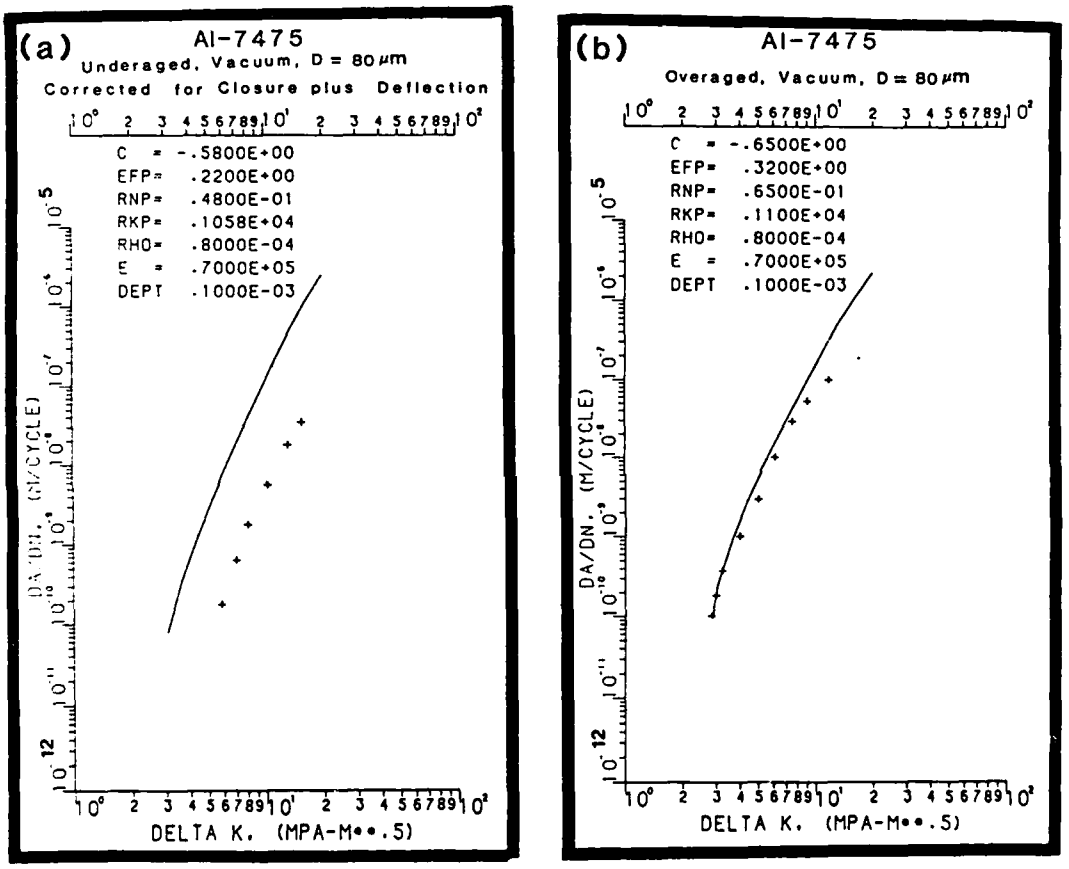

Fig. 14. Predicted and measured (+) crack growth data for 7475 (a) underaged and (b) overaged. All data corrected for closure and deflection.

Table V. Comparison of Calculated Intrinsic ΔK_{th} and Experimentally Measured Values*

Alloy Condition	Environment	ΔK_{th} (MPa $m^{\frac{1}{2}}$) calculated	ΔK_{th}^{*} (MPa $m^{\frac{1}{2}}$) experimental
Al-Zn-Mg, UA D = 15 μm	Lab Air	1.640	2.453
Al-Zn-Mg, UA D = 15 μm	Dry Air	1.648	2.586
Al-Zn-Mg, UA D = 15 μm	Vacuum	1.677	7.503
Al-Zn-Mg, OA D = 15 μm	Dry Air	1.626	1.745
Al-7475, UA D = 80 μm	Vacuum	3.169	5.655
Al-7475, OA D = 80 μm	Vacuum	2.876	2.863

* corrected for closure and crack deflection

The results of this task can be summarized as follows: The modified Chakrabortty equation includes most intrinsic contributions to the FCP resistance. The model does not include the effect of slip reversibility which may be different in the FCP-RPZ from that which occurs in a LCF specimen. In most cases, the ΔK_{th} calculated using the critical strain necessary to form PSB's was almost the same as closure-deflection-corrected measured values. In most cases, relatively good agreement was found between predicted FCGR's and closure-deflection-corrected measured values over a large ΔK range. Poor agreement existed between predicted and measured values for those conditions that allowed extensive slip reversibility, i.e., underaged specimens tested in vacuum.

C. The Effect of Ion Implantation on the Fatigue Crack Initiation Resistance of 7475

Commercially processed 7475 and the large-grained underaged 7475 described in Section II-A are being subjected to surface modification in order to improve FCI resistance. The desired microstructure in this region should enhance homogeneous deformation. A large volume fraction of nonshearable precipitates is one method of accomplishing this goal. However, normal overaging treatments or composition modifications during ingot casting are unsatisfactory since they modify bulk properties. Surface modification can be achieved by techniques such as shot peening, nitriding, plating, ion implantation and laser glazing. Of these, ion implantation has the advantage of introducing almost any ion substitutionally and interstitially into the target substrate.

Our initial studies involve the implantation of iron. Iron has adverse effects when present during ingot casting because it forms large constituent phases. However, when precipitated from the solid state, it can form very small dispersoids of Al_6Fe which are incoherent with the matrix and tend to homogenize deformation. Although iron has a very low solubility in aluminum (0.05 wt.% at RT), concentrations as large as 1% may be obtained by ion implantation. This should be sufficient to form the volume fraction of Al_6Fe necessary to homogenize deformation in the surface region. Since the equilibrium solubility is so low, and since iron has a very small diffusion coefficient in aluminum, the Al_6Fe precipitates should be relatively stable.

Fe^+ ions have been implanted into commercially processed underaged 7475 using a beam energy of 100 KeV and a flux of 5×10^{20} ions/m^2. X-ray and TEM analysis showed that the implanted surface contained a high density of small Al_6Fe dispersoids. Preliminary low cycle fatigue results indicate that the implantation significantly improves the fatigue crack initiation resistance, when compared with non-implanted samples, for strain amplitude above 0.4% plastic strain. In this regime the initiation of cracks is associated with slip bands, and the ion implantation appears to reduce the intensity of the bands. However, at low strain amplitudes no beneficial effect was observed. It appears that constituent particles control the FCI resistance at low strain amplitudes, as demonstrated by Kung and Fine (43).

Our ion implantation studies have just begun and will continue in 1984.

PROFESSIONAL PERSONNEL

Dr. E.A. Starke, Jr.
Dr. F.S. Lin
Dr. C.J. Beevers
Dr. E.W. Lee
Dr. R.T. Chen

GRADUATE STUDENTS

Dwight Janoff
R.D. Carter

PRESENTATIONS AND PUBLICATIONS UNDER AFOSR-83-0061

1. Paper presented at the 1983 TMS-AIME Annual Meeting, Atlanta, GA, March 7-10, 1983, "The Effect of Microstructure and Environment on Fatigue Crack Closure of Aluminum 7475."

2. Paper presented at the International Symposium on Concepts of Fatigue Crack Growth Threshold, Philadelphia, PA, October 2-5, 1983, "the Use of The Cyclic Stress Strain Curve and a Damage Model for Predicting Fatigue Crack Growth Thresholds."

3, R.D. Carter, E.W. Lee, E.A. Starke, Jr., and C.J. Beevers, "The Effect of Microstructure and Environment on Fatigue Crack Closure of 7475 Aluminum Alloy," Metall. Trans. A, 1984, vol. 15A, March issue.

4. E.A. Starke, Jr., F.S. Lin, R.T. Chen and H.C. Heikkenen, "The Use of the Cyclic Stress Strain Curve and a Damage Model for Predicting Fatigue Crack Growth Thresholds," to appear in the conference volume, Concepts of Fatigue Crack Growth Thresholds, David Davidson and S. Suresh, eds., to be published by the Metall. Soc. of AIME.

References

1. Cooper, Thomas D. and Clifford A. Kelto, "Fatigue in Machines and Structures-Aircraft," Fatigue and Microstructure, ASM, Metals Park, OH, 1979, p. 29.

2. John A. Wert, N.E. Paton, C.H. Hamilton, and M.W. Mahoney, Metall. Trans. A, 1981, vol. 12A, p. 1267.

3. Edgar A. Starke, Jr., in Strength of Metals and Alloys (ICSMAG), R.C. Gifkins, eds., Pergamon Press, Oxford, 1983, vol. 3, p. 1025.

4. Fu-Shiong Lin and E.A. Starke, Mat. Sci. Eng., 1980, vol. 43, p. 65.

5. J. Lindigkeit, G. Terlinde, A. Gysler, and G. Lütjering, Acta Metall., 1979, vol. 27, p. 1717.

6. J. Petit, B. Bouchet, C. Goss, and J. de Fouguet, in Fracture, Proc. 4th Int. Conf. on Fracture (ICF4), D.M.R. Taplin, ed., University of Waterloo Press, Waterloo, Canada, 1977, vol. 2, p. 867.

7. M.D. Holliday and C.J. Beevers, in Int. J. of Fracture, 1979, vol. 15, p. R27.

8. Fu-Shiong Lin and E.A. Starke, Jr., Mat. Sci. Eng., 1980, vol. 45, p. 153.

9. Fu-Shiong Lin and E.A. Starke, Jr., in Hydrogen in Metals, A.W. Thompson and I.M. Bernstein, eds., TMS-AIME, Warrendale, PA, 1981, p. 485.

10. A.K. Vasudévan and S. Suresh, Metall. Trans. A, 1982, vol. 13A, p. 2271.

11. N. Walker and C.J. Beevers, Fat. of Eng. Mat. and Struct., 1979, vol. 1, p. 135.

12. B.R. Kirby and C.J. Beevers, Fatigue of Eng. Mat. and Structures, 1979, vol. 1, p. 203.

13. S. Suresh, Metall. Trans. A, 1983, vol. 14A, p. 2375.

14. J.T. Fong, in Damage in Composite Materials, ASTM STP 775, American Society for Testing Materials, 1982, p. 243.

15. J. Lankford, D.L. Davidson and R.P. Wei, eds., Quantitative Assessment of Fatigue Damage, ASTM STP 811, American Society for Testing Materials, 1983.

16. J.C. Grosskreutz, Phys. Stat. Sol. (b), 1971, vol. 47, p. 11.

17. Campbell Laird, in Fatigue and Microstructures, M. Meshii, ed., ASM, Metals Park, OH, 1979, p. 149.

18. H. Mughrabi, in Proc. of 5th Inter. Conf. on the Strength of Metals and Alloys, Pergamon Press, Oxford, 1980, vol. 3.

19. C.J. Beevers, in Fatigue Thresholds: Fundamentals and Engineering Applications, Vol. I, J. Bäcklund, A. Blom and C.J. Beevers, eds., Engineering Materials Advisory Services, Ltd., West Midlands, UK, 1982, p. 257.

20. W. Elber, Eng. Fract. Mech., 1970, vol. 2, p. 37.

21. R.O. Ritchie and S. Suresh, Metall. Trans. A, 1978, vol. 9A, p. 291.

22. N. Walker and C.J. Beevers, Fat. of Eng. Mat. and Struct., 1979, vol. 1, p. 135.

23. R.O. Ritchie, S. Suresh and C.M. Moss, J. Eng. Mat. and Tech., Trans ASME Series H, 1979, vol. 102, p. 293.

24. S. Suresh, Metall. Trans. A, 1983, vol. 14A, p. 2375.

25. S.B. Chakrabortty, Fat. of Eng. Mat. and Struct., 1979, vol. 2, p. 331.

26. H.C. Heikkenen, E.A. Starke, Jr., and S.B. Chakrabortty, Scripta Met., 1982, vol. 16, p. 571.

27. W. Vogel, M. Wilhelm and V. Gerold, Acta Met., 1982, vol. 30, p. 31.

28. S.B. Chakrabortty and E.A. Starke, Jr., Metall. Trans. A, 1979, vol. 10A, p. 1901.

29. R.W. Hertberg and W.J. Mills, in Fractography-Microscopic Cracking Processes, ASTM STP 600, American Society for Testing Materials, 1976, p. 220.

30. C.J. Beevers, Metal Sci., 1977, vol. 11, p. 362.

31. A. Otsuka, K. Mori and T. Miyata, Eng. Fract. Mech., 1975, vol. 7, p. 429.

32. A.J. McEvily, Metal Sci., 1977, vol. 11, p. 274.

33. Herman C. Heikkenen, "A Study of the Fatigue Behavior of an Al-6Zn-2Mg-0.1Zr Alloy," M.S. Thesis, Georgia Institute of Technology, Atlanta, GA, November, 1981.

34. J. McKittrick, P.K. Liaw, S.I. Kwun and M.E. Fine, Metall. Trans. A, 1981, vol. 12A, p. 1535.

35. R.O. Ritchie, Int. Metals Rev., 1979, vol. 24, p. 205.

36. K. Minakawa and A.J. McEvily, in Fatigue Thresholds: Fundamentals and Engineering Applications, Vol. I, J. Bäcklund, A.F. Blom and C.J. Beevers, eds., Engineering Materials Advisory Services, Ltd., West Midlands, UK, 1981, p. 373.

37. J. Lindigkeit, G. Terlinde, A. Gysler and G. Lütjering, Acta Met., 1979, vol. 27, p. 1717.

38. E.O. Hall, Proc. Phys. Soc., 1951, vol. 64, p. 747.

39. N.J. Petch, J. Iron Steel Inst., 1953, vol. 197, p. 25.

40. R.B. Nicholson, in Strengthening Methods in Crystals, A. Kelly and R.B. Nicholson, eds., Applied Science Pub., Ltd., London, 1971, p. 535.

41. Alain Renard, A.S. Cheng. R. de La Vraux and C. Laird, Mat. Sci. Eng., 1983, vol. 60, p. 113.

42. M. Wilhelm, Mat. Sci. Eng., 1981, vol. 48, p. 91.

43. C.Y. Kung and M.E. Fine, Metall. Trans. A, 1979, vol. 10A, p. 603.

DISTRIBUTION LIST

Copy No.

1 - 6 Air Force Office of Scientific Research/NE
Building 410
Bolling Air Force Base
Washington, D. C. 20332

Attention: Alan H. Rosenstein

7 - 8 E. A. Starke, Jr.

9 - 10 E. H. Pancake
Clark Hall

11 RLES Files

JO# 4370 JDH

UNIVERSITY OF VIRGINIA
School of Engineering and Applied Science

The University of Virginia's School of Engineering and Applied Science has an undergraduate enrollment of approximately 1,500 students with a graduate enrollment of approximately 500. There are 125 faculty members, a majority of whom conduct research in addition to teaching.

Research is a vital part of the educational program and interests parallel academic specialties. These range from the classical engineering disciplines of Chemical, Civil, Electrical, and Mechanical and Aerospace to newer, more specialized fields of Biomedical Engineering, Systems Engineering, Materials Science, Nuclear Engineering and Engineering Physics, Applied Mathematics and Computer Science. Within these disciplines there are well equipped laboratories for conducting highly specialized research. All departments offer the doctorate; Biomedical and Materials Science grant only graduate degrees. In addition, courses in the humanities are offered within the School.

The University of Virginia (which includes approximately 1,500 full-time faculty and a total full-time student enrollment of about 16,000), also offers professional degrees under the schools of Architecture, Law, Medicine, Nursing, Commerce, Business Administration, and Education. In addition, the College of Arts and Sciences houses departments of Mathematics, Physics, Chemistry and others relevant to the engineering research program. The School of Engineering and Applied Science is an integral part of this University community which provides opportunities for interdisciplinary work in pursuit of the basic goals of education, research, and public service.